ORIGINAL PAPER

Determination of the activity of γ-glutamyl transpeptidase and of its inhibitors by using the inner filter effect on the fluorescence of nitrogen-doped carbon dots

Xia Tong[1] · Te Li[1] · Ruiqing Long[1] · Ying Guo[2] · Lihui Wu[1] · Shuyun Shi[1,2] (ORCID)

Abstract

A fluorescence (FL) probe for determination of γ-glutamyl transpeptidase (GGT) activity and evaluation of inhibitors was developed based on the inner filter effect (IFE) of nitrogen-doped carbon dots (N-CDs). Bright green emissive N-CDs were synthesized by one-step hydrothermal technique with catechol and ethylenediamine. The excitation and emission wavelengths for N-CDs were 408 and 510 nm, respectively. γ-L-Glutamyl-4-nitroanilide (γ-G4NA) was employed as the substrate of GGT. The absorption spectrum of GGT catalytic product (4-nitroaniline, 4-NA) overlapped greatly with the excitation spectrum of N-CDs. 4-NA acted as the absorber in IFE to quench the FL of N-CDs. Thus, the FL quenching of N-CDs was closely related to GGT activity. The established FL method offered good linear relationship within 2.0–10.0 U L^{-1} (R^2, 0.982) and 10.0–110.0 U L^{-1} (R^2, 0.998) with a low detection limit of 0.6 U L^{-1}. The method was successfully applied to investigate GGT activity in human serum samples with acceptable recoveries (99.1–105.0%). The approach was also employed for screening GGT inhibitors from different polar extracts of *Schisandra chinensis*. Results indicated that this strategy presents superior characteristics for GGT sensing. This method has great potential as a candidate for diagnosis of GGT-related diseases and high-throughput drug discovery.

Keywords Carbon dots · Inner filter effect · Fluorometric determination · γ-Glutamyl transpeptidase · Inhibitor

Introduction

γ-Glutamyl transpeptidase (GGT; EC 2.3.2.2) can catalyze γ-glutamyl group from glutathione (GSH) or other γ-glutamyl derivatives to amino acids and dipeptides [1]. The elevated level of GGT associates with some diseases, including pathologic states of oxidative stress, acute hepatocellular damage, diabetes, and cancers [1–3]. Therefore, in order to diagnose GGT-related diseases, a sensitive and accurate strategy to determine GGT activity in vitro and in vivo is urgently needed. To date, many methods have been applied to assay GGT activity including high-performance liquid chromatography (HPLC) [4], colorimetric assays [5, 6], electrochemistry [7], surface-enhanced Raman spectroscopy (SERS) [8], and fluorescence (FL) sensing [9–11]. Notably, FL methods can reduce the effect of background noise and improve sensitivity, and lots of organic FL probes have been designed to monitor GGT activity [11]. However, professional knowledge for multistep synthesis and potential toxicity of organic sensors may affect their development [12].

Carbon dots (CDs) had gained considerable attention in biosensing and bioimaging due to their convenient preparation, chemical stability, low toxicity, and high biocompatibility [13, 14]. CDs have been well fabricated and utilized to sense pH [15], ions [16], organic pollutants [17], and biological molecules [18, 19]. Among them, CD-based FL assays of

✉ Ying Guo
  guoying881212@csu.edu.cn

✉ Shuyun Shi
  shuyshi@csu.edu.cn

[1] Key Laboratory of Hunan Province for Water Environment and Agriculture Product Safety, College of Chemistry and Chemical Engineering, Central South University, Changsha 410083, People's Republic of China

[2] Department of Clinical Pharmacology, Xiangya Hospital; Hunan Key Laboratory of Pharmacogenetics, Central South University, 410078 Changsha, People's Republic of China

enzyme activities were still a challenging task due to the fabrication of suitable fluorophore–quencher pair to ensure effective detection. Tang et al. assayed alkaline phosphatase (ALP) activity based on β-cyclodextrin–modified CDs through host–guest recognition of ALP catalytic product and its photoinduced electron transfer (PET) with CDs [20]. Chang et al. designed a fluorescent turn-on biosensor based on fluorescence resonance energy transfer (FRET) from GSH functionalized Mn-doped ZnS quantum dots to graphene oxide to determine glutathione S-transferase [21]. FL probes based on inner filter effect (IFE) between enzyme catalytic products and CDs were fabricated for determination of α-glucosidase [22, 23], β-glucuronidase [24, 25], xanthine oxidase [26], alkaline phosphatase [27], and cholinesterase [28] activities. IFE occurs if the absorption spectra of absorbers overlap with the excitation or emission spectra of fluorophores [22]. Compared with other sensing mechanisms, IFE does not require complex operation processes or CD functionalization. IFE has shown enhanced sensitivity of FL probes than pure absorption methods by transforming absorbance signals to FL signals [25]. However, to our best knowledge, there is no report about IFE-based FL probes to sense GGT activity. GGT inhibitors, from natural products due to their multitarget therapy, curative effect, and less side effect, may be explored as anticancer candidates. Therefore, it is still necessary to develop a sensitive and rapid platform for GGT activity detection and its inhibitor evaluation.

Here, an effective and sensitive FL probe for GGT assay and its inhibitor evaluation was fabricated using nitrogen-doped carbon dots (N-CDs) based on IFE. N-CDs with bright green emission at 510 nm under 408-nm excitation were synthesized by hydrothermal treatment of catechol and ethylenediamine. γ-L-Glutamyl-4-nitroanilide (γ-G4NA) was chosen as the GGT-specific substrate. Through GGT catalysis, 4-nitroanilide (4-NA) was released and functioned as the absorber in IFE to turn off the FL of N-CDs, due to the good overlap between absorption of 4-NA (381 nm) and excitation spectrum of N-CDs (Scheme 1). The FL sensor can not only be applied to assay GGT activity but also screen the GGT inhibitors from natural products. This strategy possessed many merits including excellent selectivity, high sensitivity, and low toxicity which showed great potential for clinic diagnosis and drug discovery.

Materials and methods

Reagents and instruments

γ-Glutamyl transpeptidase (GGT; EC 2.3.2.2) from bovine kidney was purchased from Yuanye Bio-Technology Co., Ltd. (Shanghai, China, http://www.shyuanye.com). γ-L-Glutamyl-4-nitroanilide (γ-G4NA) was bought from Alfa

Aesar (Shanghai, China, https://www.alfa.com). Glycylglycine (Gly-Gly), 4-nitroanilide (4-NA), and catechol were supplied by Energy Chemical Co., Ltd. (Shanghai, China, https://www.energy-chemical.com). Ethylenediamine, $FeCl_3$, KCl, $CaCl_2$, NaCl, $Cu(NO_3)_2$, $Zn(NO_3)_2$, and $MgSO_4$ were provided by Sinopharm Chemical Reagent Co., Ltd. (Beijing, China, http://en.reagent.com.cn). L-Histidine (L-His), L-phenylalanine (L-Phe), L-leucine (L-Leu), L-serine (L-Ser), L-cysteine (L-Cys), L-glycine (L-Gly), L-isoleucine (L-Lle), L-proline (L-Pro), L-threonine (L-Thr), L-valine (L-Val), glutathione (GSH), and schizandrin A were obtained from Aladdin Reagent Co., Ltd. (Shanghai, China, https://aladdin-e.com). Ultrapure water was obtained through 18.25 MΩ cm by Molecular water purification system (http://www.chem17.com/st172141/). Phosphate-buffered saline (PBS) powder (pH 7.2–7.4) was brought from Solarbio (Beijing, China, http://www.Solarbio.com). The PBS solution (10 mM) was prepared by water dilution, which contained NaCl (137 mM) , Na_2HPO_4 (8 mM), and NaH_2PO_4 (2 mM). All reagents were of analytical grade and used without further purification.

Morphologies and sizes were characterized by a HT7700 transmission electron microscope (TEM, Hitachi, Japan, https://www.hitachi.com) with an accelerating voltage of 200 kV. X-Ray photoelectron spectroscopy (XPS) was obtained with Escalab Xi+ (Thermo Fisher Scientific, USA, https://www.thermofisher.com/cn/zh/home.html). X-Ray diffraction (XRD) was performed on Empyrean (PANalytical, Netherlands, https://www.malvernpanalytical.com/en/). Ultraviolet-visible (UV-vis) absorption spectra were conducted on a UV-2600 UV-vis spectrophotometer (Shimadzu, Japan, https://www.shimadzu.com). Fourier-transform infrared spectra (FT-IR) were measured by Spectrum Two (PerkinElmer Ltd., USA, https://www.perkinelmer.com.cn). FL decay time curves were collected on a FluoTime 100 spectrofluorometer (PicoQuant, Germany, https://www.picoquant.com). FL spectra were recorded with a LS-55 spectrofluorometer (PerkinElmer Ltd., USA, https://www.perkinelmer.com.cn) with a voltage of 740 V under 408-nm excitation, wavelength range of 430–650 nm, and slit widths of 10 nm and 15 nm for excitation and emission, respectively.

Preparation of N-CDs

Detailed procedures for preparation of N-CDs are shown in Electronic Supporting Material (ESM).

IFE-based FL detection of GGT activity

FL assay for GGT activity was performed as follows. Briefly, a series of GGT solutions from 0 to 150 U L^{-1} containing γ-G4NA (0.75 mM) and Gly-Gly (16.7 mM) were prepared in PBS (10 mM, pH 7.4). After shaking and incubation at 37 °C for 35 min, mixtures (20 μL) were added with N-CD solution

Scheme 1 Schematic representation of fluorometric determination of the activity of γ-glutamyl transpeptidase (GGT) and its inhibitors by using inner filter effect (IFE) of nitrogen-doped carbon dots (N-CDs)
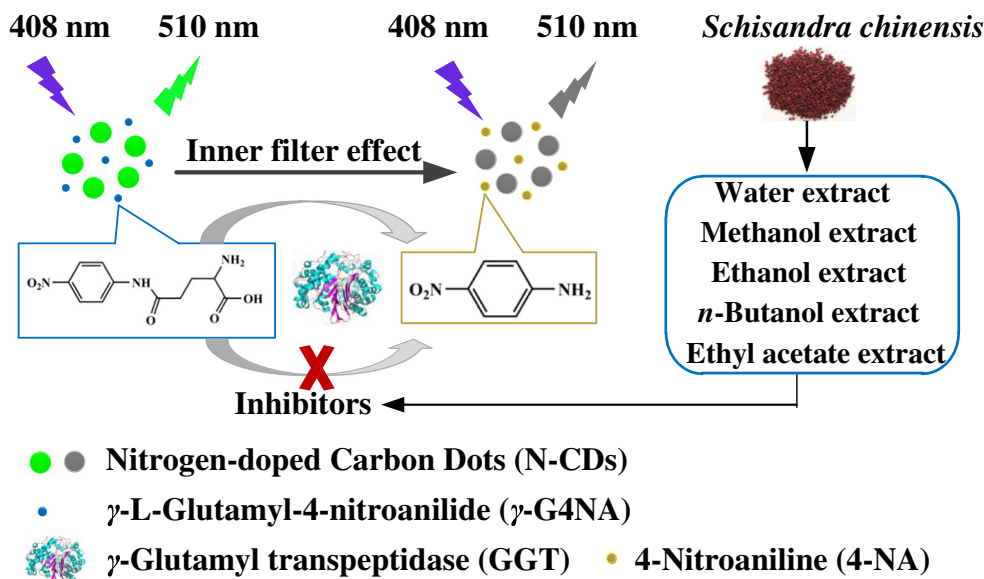
(200 μL, 0.14 mg mL^{-1}). Then, the solution was incubated for another 1.0 min at room temperature, and FL intensity was measured at 510 nm with excitation wavelength at 408 nm. The negative control experiment was processed with increasing concentrations of deactivated GGT. The deactivated GGT was obtained by being heated at 100 °C for 30 min. Possible interferents were also investigated including other enzymes, amino acids, and metal ions. Activities of glucose oxidase (GOx), α-glucosidase, ALP, and coenzyme A (CoA) were set at 5000 U L^{-1}. Concentrations of amino acids (L-His, L-Phe, L-Leu, L-Ser, L-Cys, L-Gly, L-Ile, L-Pro, L-Thr, L-Val), GSH, and metal ions (Fe^{3+}, Cu^{2+}, Mg^{2+}, Zn^{2+}, Na$^+$, K$^+$, Ca^{2+}) were all at 500 μM.

GGT inhibitor investigation

Schisandra chinensis was bought from a local drugstore (Changsha, China), which was identified by Prof. Mijun Peng, Guangdong Institute of Analysis, Guangzhou, China. Voucher specimen (SC201905) was stored at College of Chemistry and Chemical Engineering, Central South University, Changsha, Hunan, China.

S. chinensis was dried, crushed, and sieved (500 mesh). Powdered samples (100.0 g) were divided into five parts (20 g per part). The five parts were immersed with water, methanol, ethanol, *n*-butanol, and ethyl acetate, separately. After supersonic extraction for 120 min at 70 °C, the supernatant was filtered and dried under reduced pressure to achieve water extract (391.0 mg), methanol extract (30.4 mg), ethanol extract (30.1 mg), *n*-butanol extract (72.5 mg), and ethyl acetate extract (22.7 mg). Different concentrations of extracts containing GGT (50 U L^{-1}), γ-G4NA (0.75 mM), and Gly-Gly (16.7 mM) were incubated for 35 min at 37 °C. After that, reaction solution (20 μL) was

introduced into N-CD solution (200 μL, 0.14 mg mL^{-1}) for FL assay to evaluate inhibition efficiency.

GGT activity assay in human serum samples

Human serum samples were collected from adult volunteers at School Hospital of Central South University and stored frozen before use. The assays of GGT in human serum samples were processed as follows. In brief, serum samples (100 μL) were mixed with γ-G4NA (1 mM, 300 μL) and Gly-Gly (400 mM, 16.7 μL). After shaking and incubation at 37 °C for 35 min, mixtures (20 μL) were taken out and incubated with N-CD solution (200 μL, 0.14 mg mL^{-1}) for another 1.0 min at room temperature. Then, the FL intensity was measured at 510 nm with excitation wavelength at 408 nm. In recovery tests, for human serum sample 1 three levels of GGT at 2.0, 50.0, and 90.0 U L^{-1} were added, whereas for human serum sample 2, three levels of GGT at 5.0, 40.0, and 70.0 U L^{-1} were added.

Results and discussions

Choice of materials

N-CDs with prominent optical properties and functional groups present advantages including photostability, water solubility, and good biocompatibility, which then present outstanding advantages in biosensing. When the excitation spectrum of N-CDs overlaps the absorption spectrum of GGT hydrolysate 4-NA, IFE happens between N-CDs and 4-NA. Then, the GGT activity can be determined. The maximum absorption wavelength of 4-NA is about 381 nm. Notably, catechol and ethylenediamine, two common chemicals as carbon and nitrogen sources, can be hydrothermally treated to

prepare N-CDs with maximum excitation wavelength at about 400 nm [25]. Then, catechol and ethylenediamine were selected to prepare N-CDs. As depicted in Fig. S1 (ESM), the highest FL intensity is acquired when the molar ratio of catechol and ethylenediamine is 1:1.8, reaction time is 10 h, and hydrothermal reaction temperature is 180 °C.

Characterization of N-CDs

TEM image confirms that N-CDs with good monodispersion and narrow size distribution (1.0–2.2 nm) have been successfully synthesized (Fig. 1a). Element components and surface function groups of N-CDs have been analyzed by XPS and FT-IR. As seen in Fig. 1b, full-range XPS of N-CDs emerges with three major peaks at 284.8 (C1s), 399.1 (N1s), and 531.7 eV (O1s). In C1s spectrum (Fig. S2A, ESM), peaks at around 284.2, 285.1, 286.3, and 288.8 eV are attributed to C=C, C–C, O=C–O, and C=O groups, respectively [22]. Peaks at 399.0 and 400.8 eV correspond to $(C)_3$-N and N–H groups in N1s spectrum (Fig. S2B, ESM), respectively, and indicate the existence of nitrogen [25]. In Fig. 1c, FT-IR spectrum has been performed to identify functional groups of N-CDs, and broad absorption bond at 3300 cm^{-1} belongs to O–H and N–H stretching vibrations. The peak at 1630 cm^{-1} is ascribed to C=C stretching of polycyclic aromatic hydrocarbons. C=N, C–N, and C–N= stretching bands appear at 1494, 1386, and 1335 cm^{-1}, respectively. Absorption bonds emerge at 1230 and 1085 cm^{-1} corresponding to C–O stretching vibration and C–O–C stretching, respectively [22, 26]. UV-vis spectrum of N-CDs exhibits two bands at 270 ($\pi \rightarrow \pi^*$ transition of aromatic C=C bonds) and 410 nm ($n \rightarrow \pi^*$ transition of carbonyl or amine groups) (Fig. 1d) [25]. Excitation and emission wavelengths of N-CDs are 408 and 510 nm, respectively (Fig. 1d). In addition, XRD pattern of N-CDs shows one peak at around $2\theta = 21°$ (Fig. S2C, ESM), which corresponds to the (002) lattice plane, and is consistent with the result in previous reports of N-CDs [25]. In Fig. S2D (ESM), FL spectra of N-CDs display strong emission at around 510 nm by different wavelengths from 348 to 438 nm. Emission spectra are nearly independent of excitation spectra, which indicates that the sizes of N-CDs are relatively uniform [24]. Quantum yield (QY) of N-CDs is 30.5% by using quinine sulfate as the reference (QY measurement method was presented in ESM).

FL sensing mechanism of GGT activity based on IFE

IFE is due to the absorbers absorbing the excitation or emission energy of fluorophores in the detection system, and then leads to the quenching of FL intensity. In this study, γ-G4NA is employed as substrate of GGT. When GGT is introduced into mixtures of γ-G4NA and Gly-Gly, the γ-glutamyl group will be transferred from γ-G4NA to Gly-Gly and hydrolysate product of
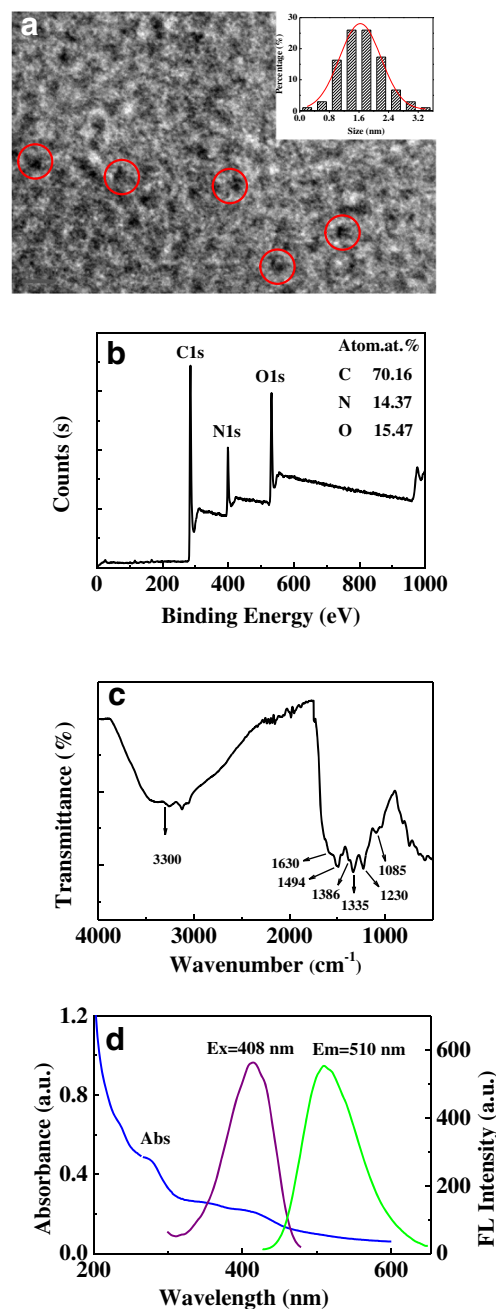
Fig. 1 **a** TEM image of N-CDs (inset, particle size distribution of N-CDs); **b** XPS survey spectrum of N-CDs; **c** FT-IR spectrum of N-CDs; **d** UV-vis absorption spectrum of N-CDs, and the excitation and emission spectra of N-CDs

4-NA is released [29]. 4-NA acts as an absorber and N-CDs serve as fluorophores in IFE. As shown in Fig. 2a, maximum absorption of γ-G4NA is at 318 nm, and the influence on FL intensity of N-CDs can be neglected (Fig. 2b). The absorption peak at 381 nm of 4-NA overlaps greatly with the excitation spectrum of N-CDs at 408 nm, reducing the FL intensity of N-CDs at 510 nm. By the IFE-based process, the absorbance signals are transformed to FL signals to improve the selectivity, sensitivity, and rapid assay for GGT activity. In addition, FL
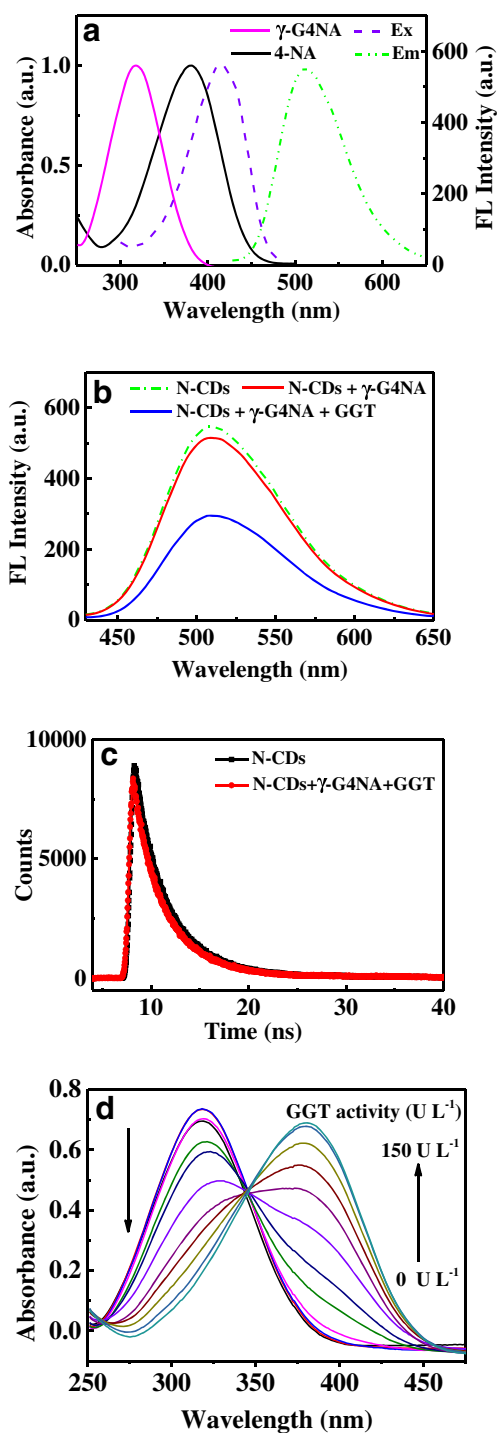
◀ **Fig. 2** **a** UV-vis absorption spectra of γ-G4NA, 4-NA, and FL excitation and emission spectra of N-CDs; **b** The change of FL spectra of N-CDs in the presence of mere N-CDs, N-CDs + γ-G4NA (0.75 mM), and N-CDs + γ-G4NA (0.75 mM) + GGT (110 U L^{-1}); **c** the FL decay curves of N-CDs in the absence and presence of reaction solution of γ-G4NA (0.75 mM) + GGT (110 U L^{-1}); **d** UV-vis absorption spectra of enzyme reaction solutions on various activities of GGT (0–150.0 U L^{-1}); **e** photograph of enzyme reaction solutions with different levels of GGT activity. F_0 and F were the FL intensity of N-CDs in the absence and presence of GGT reaction solution, respectively

lifetime can provide quenching evidence for IFE-based. Figure 2c shows that the FL lifetimes of N-CDs are 3.97 and 3.96 ns in the absence or presence of reaction solution of γ-G4NA and GGT, respectively, and are almost unchanged. Hence, FL quenching is not due to FRET or dynamic quenching [26, 30]. To investigate the quenching behavior of 4-NA on FL of N-CDs, the Stern–Volmer equation can be employed (ESM). As shown in Fig. S3 (ESM), F_0/F shows a good linear relationship ($F_0/F = 0.016 \ c_q + 1.03$) with 4-NA concentration. In this case, the value of K_q is calculated to be 4.03×10^{12} M^{-1}S^{-1}. The quenching mechanism is static quenching because K_q is larger than 1.00×10^{10} M^{-1}S^{-1} [16]. Subsequently, the contribution of IFE was estimated according to the absorption characteristics of N-CDs and 4-NA (ESM). As described in Fig. S4 (ESM), IFE is the major quenching mechanism with the increase of 4-NA concentration.

Furthermore, UV-vis absorption spectra of γ-G4NA being a hydrolysate with GGT have been analyzed. As shown in Fig. 2d, UV-vis absorbances at 318 nm and 381 nm were gradually decreasing and increasing, respectively, with GGT activity ranging from 0 to 150.0 U L^{-1}. The colors of the reaction solutions change obviously from colorless to pale yellow due to the formation of 4-NA (Fig. 2e). Colorimetric assay, which is based on the color change of 4-NA driven by GGT, is still being employed for commercial GGT assay kits [10]. However, it usually shows lower sensitivity and is less discriminatory than FL methods [31]. By employing IFE-based FL sensor, a sensitive approach for monitoring GGT hydrolysate reaction had been developed.

FL assay for GGT activity

To establish a highly specific sensor for GGT, the main influence conditions on GGT activity have been investigated, such as concentrations of N-CDs, pH of reaction solution, temperature, enzyme reaction time, and incubation time. Various N-CD concentrations (0.06, 0.10, 0.14, 0.18, and 0.22 mg mL^{-1}) have been mixed with reaction solution of γ-G4NA (0.75 mM), Gly-Gly (16.7 mM), and GGT (50.0 U L^{-1}). Results show that when concentration of N-CDs is 0.14 mg mL^{-1}, FL intensity and quenching efficiency are the highest (Fig. 3a). The influence of PBS buffer with various pH (6.5–8.0) has been evaluated. As
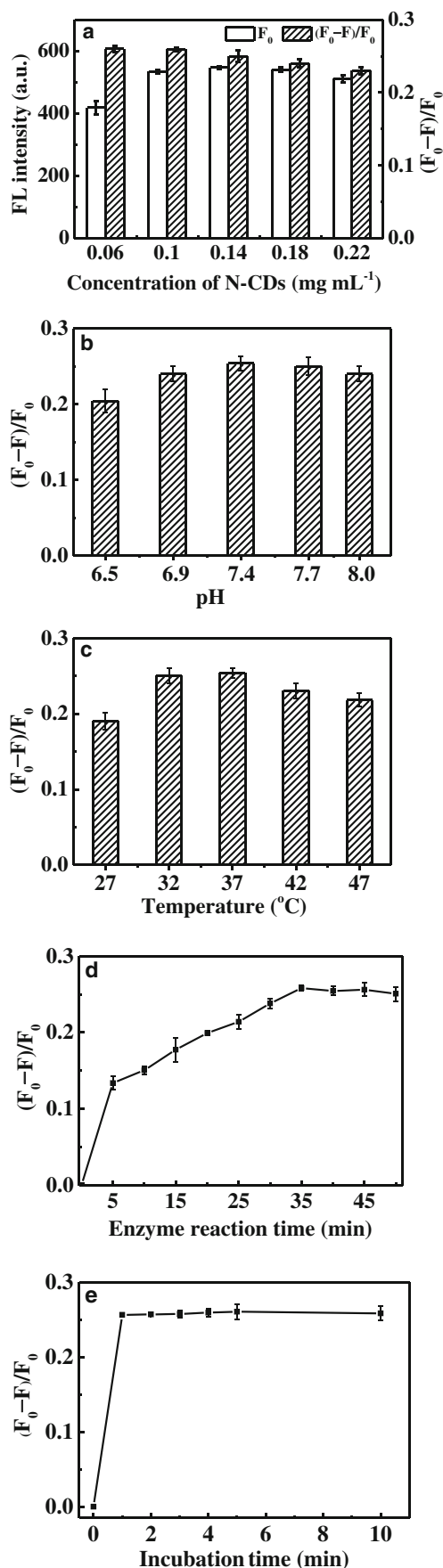
◀ **Fig. 3** The influence conditions including **a** concentration of N-CDs, **b** pH of PBS buffer, **c** reaction temperature, **d** enzyme reaction time, and **e** incubation time on FL quenching efficiency of N-CDs for GGT activity assay. F_0 and F were the FL intensity of N-CDs in the absence and presence of GGT reaction solution, respectively. Error bar represents the standard deviation ($n = 3$)

seen in Fig. 3b, pH at 7.4 gives the highest FL quenching efficiency, which is suitable for biological applications. Several reaction temperatures (27–47 °C) have also been investigated, and temperature at 37 °C yields the maximum FL quenching efficiency (Fig. 3c). As shown in Fig. 3d, studies on GGT reaction time with substrates show a fast hydrolysis process and FL quenching efficiency reaches an approximate plateau within 35 min. So, 35 min is selected as the optimal enzyme reaction time. Incubation time between reaction solution and N-CDs has also been assayed in Fig. 3e. As reaction time prolongs, FL quenching efficiency tends to level off after 1.0 min, so 1.0 min was used as the incubation time.

Under optimal conditions, FL response of N-CDs to GGT at different activities has been measured. As shown in Fig. 4a, FL intensity of N-CDs decreases with increasing GGT activity, and there is a good linear relationship between FL quenching efficiency ($(F_0-F)/F_0$) (y) and GGT activity (x) in the range 2.0–10.0 ($y = 0.007x - 0.001$, R^2 0.982) and 10.0–110.0 U L^{-1} ($y = 0.004x +$
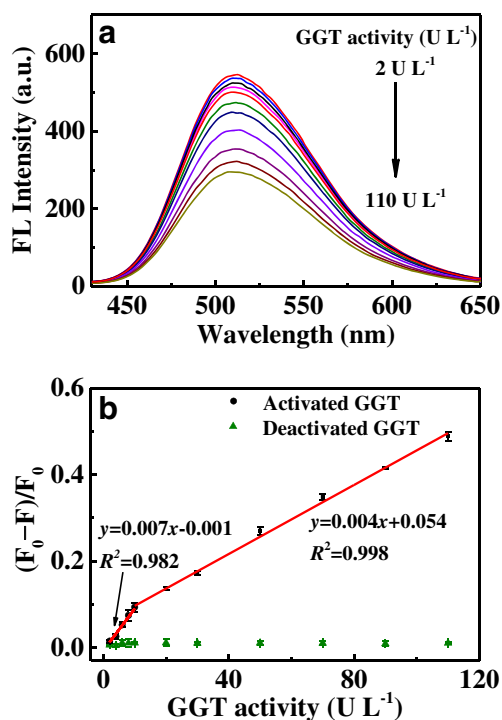

Fig. 4 **a** FL spectra of N-CDs after addition of different activities of GGT (2.0–110.0 U L^{-1}), respectively; **b** linear fitting curve of FL quenching efficiency to the GGT activities from 2.0–10.0 U L^{-1} and 10.0–110.0 U L^{-1}. Error bar represents the standard deviation ($n = 3$)

0.054, R^2 0.998) (Fig. 4b), respectively. The detection limit ($3\sigma/S$, σ is the standard deviation of blank samples, $n = 12$, and S is the slope of linear equation) is estimated to be 0.6 U L^{-1}. The linear range and LOD were enough to directly monitor the GGT levels in human serum, since the normal GGT activity is 5.0–55.0 U L^{-1} and 15.0–85.0 U L^{-1} for adult females and males, respectively [10, 31]. Furthermore, the FL-based method has comparable or contains a wider linear detection range than reported methods (Table 1). As shown in Fig. S5 (ESM) and Fig. 4b, the FL intensity and quenching efficiency are kept stable with increasing concentration of deactivated GGT.

We also investigate the selectivity of N-CDs toward some biological substances including amino acids (L-His, L-Phe, L-Leu, L-Ser, L-Cys, L-Gly, L-Lle, L-Pro, L-Thr, L-Val), biothiol (e.g., GSH), metal ions (e.g., Fe^{3+}, Cu^{2+}, Mg^{2+}, Zn^{2+}, Na^+, K^+, Ca^{2+}), and enzymes (e.g., GOx, α-Glu, ALP, CoA). As shown in Fig. 5, negligible interference on N-CDs FL quenching efficiency is observed. In Fig. S6 (ESM), FL intensities of N-CDs are nearly invariable when concentration of NaCl reaches up to 800 mM. It guarantees the favorable capability of N-CDs in selectivity of ions for biological analysis. N-CDs exhibit excellent selectivity for GGT, which may due to the specific cleavage of γ-glutamyl group in γ-G4NA by GGT [32].

Evaluation of GGT inhibitors

Natural products are abundant, have relatively less side effects in clinical usage, and may be important sources with greater inhibition of GGT activity. *S. chinensis* is an effective medicinal plant in anti-hepatitis B virus activity and alleviating liver damage [33], and is a hepatitis therapeutic [34]. Lignans in *S. chinensis* can decrease GGT levels significantly [33]. Herein, schizandrin A (positive control), water extract, methanol extract, ethanol extract, *n*-butanol extract, and ethyl acetate extract of *S. chinensis* have been employed to evaluate GGT inhibitory activities. With introduction of GGT inhibitors, the activity of GGT hydrolysis of γ-G4NA to 4-NA can be restricted, and then the IFE is reduced. Then, FL quenching of N-CDs can be recovered depending on the concentration of
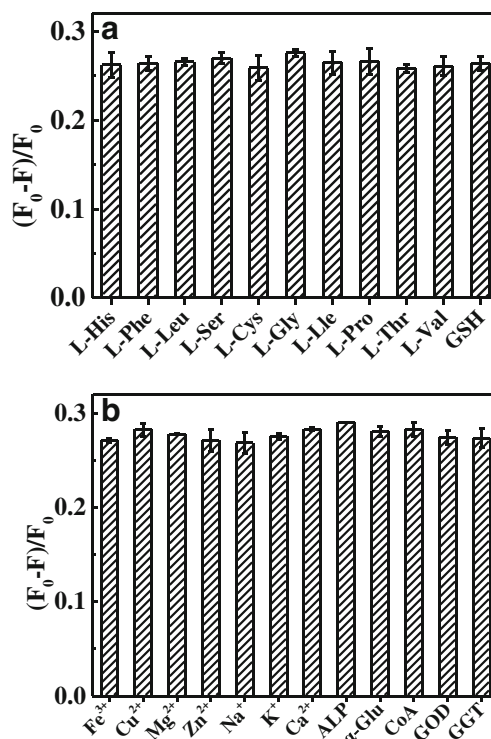

Fig. 5 **a** FL responses of N-CDs to some amino acids and GSH; **b** FL responses of N-CDs toward several metal ions, ALP, α-Glu, CoA, GOx, and GGT. The concentrations of amino acids, metal ions, and GSH were 500 mM, the activity of ALP, α-Glu, CoA, and GOx were 5000 U L^{-1}, and the activity of GGT was 50.0 U L^{-1}. F_0 and F were the FL intensity of N-CDs in the absence and presence of the interfering substances, respectively. Error bar represents the standard deviation ($n = 3$)

inhibitors. The inhibiting efficiency is expressed by inhibition ratio (I (%)), and the equation is:

$$I\ (\%) = (F_I - F_0)/(F_B - F_0) \times 100$$

where F_I is the FL intensity in the presence of GGT inhibitors, F_0 stands for the FL intensity in the presence of GGT without inhibitors as blank reference, and F_B is the initial FL intensity of N-CDs, γ-G4NA, and Gly-Gly without GGT as control reference. Sample concentration providing 50% inhibition (IC_{50}) is calculated from the graph plotting inhibition percentage. Figure S7 (ESM) presents that FL intensity of N-CDs is enhanced with increasing concentration of schizandrin A, indicating the inhibition of the activity of GGT. IC_{50} value of

Table 1 Comparisons of reported strategies for GGT activity assay

Methods	Linear range (U L^{-1})	LOD (U L^{-1})	References
Colorimetric method	0.18–4	–[a]	[6]
Surface-enhanced Raman spectroscopy	0.2–200	0.09	[8]
Two-photon fluorescent probe	1–35	0.057	[9]
Ratiometric fluorescent probe	0–50	0.76	[10]
N-CD–based fluorescence method	2.0–10.0	0.6	This work
	10.0–110.0		

[a] Not detected

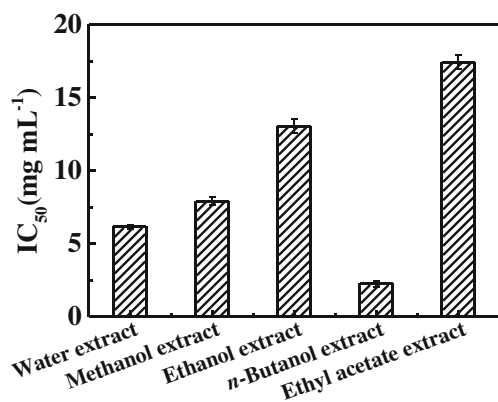**Fig. 6** IC_{50} values of water extract, methanol extract, ethanol extract, *n*-butanol extract, and ethyl acetate extract of *S. chinensis* on GGT

schizandrin A is calculated to be 0.155 mg mL^{-1}. For different extracts, the IC_{50} values of water extract, methanol extract, ethanol extract, *n*-butanol extract, and ethyl acetate extract of *S. chinensis* are 6.2, 7.9, 13.1, 2.3, and 17.4 mg mL^{-1}, respectively (Fig. 6, and Fig. S8, ESM). Obviously, *n*-butanol extract with polar components is rich of GGT inhibitors, which deserves further preparative isolation and structural elucidation. The results demonstrate that the method can be employed to screen GGT inhibitors from natural products for new drug discovery.

Human serum sample detection

As we know, the activity of human serum GGT is a biomarker in diagnosing diseases, for instance, hepatitis, alcoholic liver injury, and liver cancer. Here, we attempt to assay GGT activity in human serum to verify the practicality and reliability of the strategy based on N-CDs. As shown in Table 2, GGT activities in healthy serum samples are 9.7 and 24.3 U L^{-1}, respectively, which are in the range of normal GGT activity. In addition, by the traditional colorimetric method, GGT activities in healthy serum samples are determined to be 8.3 and 25.4 U L^{-1}. The fluorometric and colorimetric agreed very

Table 2 Recovery results of the determination of GGT in human serum samples

samples	Spiked (U L^{-1})	Found (U L^{-1})	Recoveries (%)	RSD ($n = 3$, %)
Sample 1	0	9.7 ± 0.12	–	0.8
	2.0	11.8 ± 0.12	105.0	2.9
	50.0	59.1 ± 0.54	98.8	1.8
	90.0	99.2 ± 2.1	99.4	2.0
Sample 2	0	24.3 ± 0.13	–	1.1
	5.0	29.5 ± 0.54	104.0	2.5
	40.0	64.2 ± 0.46	99.8	1.4
	70.0	93.7 ± 1.73	99.1	3.2

well. After spiking different activities of standard GGT, recoveries are 99.1–105.0% and relative standard deviations (RSD) are 0.8–3.2%. It indicated that this FL probe has great potential for detection of GGT levels in human serum in clinical studies.

Conclusions

In summary, we have, for the first time, developed a FL probe for GGT activity monitoring and evaluation of its inhibitors based on IFE of N-CDs. γ-G4NA is chosen as a specific substrate of GGT due to the hydrolysis product; 4-NA is the absorber in IFE, while in N-CDs, it is the IFE fluorophore. This method also has been applied to GGT assay of human serum samples. In addition, it can be applied as a new tool for screening GGT inhibitors from natural products for new drug discovery. In the future, this strategy can be expanded to detect other important enzymes in bioanalysis. However, this method also has limitations (e.g., long synthesis time). Thus, we aim to simplify the preparation process of CDs to determine GGT more conveniently in the future.

Compliance with ethical standards

Conflict of interest All the authors declare no conflict of interest.

References

1. Castellano I, Merlino A, Rossi M, La Cara F (2010) Biochemical and structural properties of gamma-glutamyl transpeptidase from Geobacillus thermodenitrificans: an enzyme specialized in hydrolase activity. Biochimie 92:464–474

2. Pompella A, De Tata V, Paolicchi A, Zunino F (2006) Expression of γ-glutamyltransferase in cancer cells and its significance in drug resistance. Biochem Pharmacol 71:231–238

3. Choi YJ, Lee DH, Han K-D, Yoon H, Shin CM, Park YS, Kim N (2017) Elevated serum gamma-glutamyltransferase is associated with an increased risk of oesophageal carcinoma in a cohort of 8,388,256 Korean subjects. PLoS One 12:0177053–0177064

4. Kiuchi K, Nagatsu T, Togari A, Kumagai H (1986) Highly sensitive assay for γ-glutamyltranspeptidase activity by high-performance liquid chromatography with electrochemical detection. J Chromatogr A 357:191–198

5. Orlowski M, Meister A (1963) γ-Glutamyl-*p*-nitroanilide: a new convenient substrate for determination and study of L- and D-γ-glutamyltranspeptidase activities. Biochim Biophys Acta 73:679–681

6. Del Corso A, Cappiello M, Buono F, Moschini R, Paolicchi A, Mura U (2006) Colorimetric coupled enzyme assay for γ-

glutamyltransferase activity using glutathione as substrate. J Biochem Biophys Methods 67:123–130

7. Chen G, Ni S, Zhu S, Yang J, Yin Y (2012) An electrochemical method to detect gamma glutamyl transpeptidase. Int J Mol Sci 13: 2801–2809

8. Jiang L, Guo D, Wang L, Chang S, Li J, Zhan D, Fodjo EK, Gu H, Li D (2019) Sensitive and selective SERS probe for detecting the activity of γ-glutamyl transpeptidase in serum. Anal Chim Acta DOI. https://doi.org/10.1016/j.aca.2019.11.041

9. Zhang P, Jiang X, Nie X, Huang Y, Zeng F, Xia X, Wu S (2016) A two-photon fluorescent sensor revealing drug-induced liver injury via tracking γ-glutamyltranspeptidase (GGT) level *in vivo*. Biomaterials 80:46–56

10. Hou X, Yu Q, Zeng F, Yu C, Wu S (2014) Ratiometric fluorescence assay for γ-glutamyltranspeptidase detection based on a single fluorophore via analyte-induced variation of substitution. Chem Commun 50:3417–3420

11. Luo Z, An R, Ye D (2019) Recent advances in the development of optical imaging probes for γ-Glutamyltranspeptidase. Chem Bio Chem 20:474–487

12. Das RK, Mohapatra S (2017) Highly luminescent, heteroatom-doped carbon quantum dots for ultrasensitive sensing of glucosamine and targeted imaging of liver cancer cells. J Mater Chem B 5:2190–2197

13. Yang Z, Xu M, Liu Y, He F, Gao F, Su Y, Wei H, Zhang Y (2014) Nitrogen-doped, carbon-rich, highly photoluminescent carbon dots from ammonium citrate. Nanoscale 6(3):1890–1895

14. Wang L, Zhou HS (2014) Green synthesis of luminescent nitrogen-doped carbon dots from milk and its imaging application. Anal Chem 86(18):8902–8905

15. Shangguan J, He D, He X, Wang K, Xu F, Liu J, Tang J, Yang X, Huang J (2016) Label-free carbon-dots-based ratiometric fluorescence pH nanoprobes for intracellular pH sensing. Anal Chem 88(15):7837–7843

16. Li T, Xie L, Long R, Tong C, Guo Y, Tong X, Shi S, Lin Q (2019) Cetyltrimethyl ammonium mediated enhancement of the red emission of carbon dots and an advanced method for fluorometric determination of iron(III). Microchim Acta 186(12):791–798

17. Li Y, Liu X, Wu Q, Yi J, Zhang G (2018) Discrimination and detection of benzaldehyde derivatives using sensor array based on fluorescent carbon nanodots. Sens Actuators B: Chem 261:271–278

18. Pirsaheb M, Mohammadi S, Salimi A, Payandeh M (2019) Functionalized fluorescent carbon nanostructures for targeted imaging of cancer cells: a review. Microchim Acta 186:231–240

19. Long R, Guo Y, Xie L, Shi S, Xu J, Tong C, Lin Q, Li T (2020) White pepper-derived ratiometric carbon dots for highly selective detection and imaging of coenzyme A. Food Chem DOI. https://doi.org/10.1016/j.foodchem.2020.126171

20. Tang C, Qian Z, Huang Y, Xu J, Ao H, Zhao M, Zhou J, Chen J, Feng H (2016) A fluorometric assay for alkaline phosphatase activity based on β-cyclodextrin-modified carbon quantum dots through host-guest recognition. Biosens Bioelectron 83:274–280

21. Chang L, He X, Chen L, Zhang Y (2017) A novel fluorescent turn-on biosensor based on QDs@ GSH–GO fluorescence resonance energy transfer for sensitive glutathione S-transferase sensing and cellular imaging. Nanoscale 9:3881–3888

22. Li G, Kong W, Zhao M, Lu S, Gong P, Chen G, Xia L, Wang H, You J, Wu Y (2016) A fluorescence resonance energy transfer (FRET) based "turn-on" nanofluorescence sensor using a nitrogen-doped carbon dot-hexagonal cobalt oxyhydroxide nanosheet architecture and application to α-glucosidase inhibitor screening. Biosens Bioelectron 79:728–735

23. Huang S, Yang E, Yao J, Liu Y, Xiao Q (2018) Carbon dots doped with nitrogen and boron as ultrasensitive fluorescent probes for determination of α-glucosidase activity and its inhibitors in water samples and living cells. Microchim Acta 185:394–403

24. Gong P, Sun L, Wang F, Liu X, Yan Z, Wang M, Zhang L, Tian Z, Liu Z, You J (2019) Highly fluorescent N-doped carbon dots with two-photon emission for ultrasensitive detection of tumor marker and visual monitor anticancer drug loading and delivery. Chem Eng J 356:994–1002

25. Lu S, Li G, Lv Z, Qiu N, Kong W, Gong P, Chen G, Xia L, Guo X, You J (2016) Facile and ultrasensitive fluorescence sensor platform for tumor invasive biomaker β-glucuronidase detection and inhibitor evaluation with carbon quantum dots based on inner-filter effect. Biosens Bioelectron 85:358–362

26. Tang D, Zhang J, Zhou R, Xie Y, Hou X, Xu K, Wu P (2018) Phosphorescent inner filter effect-based sensing of xanthine oxidase and its inhibitors with Mn-doped ZnS quantum dots. Nanoscale 10: 8477–8482

27. Mao M, Tian T, He Y, Ge Y, Zhou J, Song G (2017) Inner filter effect based fluorometric determination of the activity of alkaline phosphatase by using carbon dots codoped with boron and nitrogen. Microchim Acta 185:17–22

28. Xu X, Cen Y, Xu G, Wei F, Shi M, Hu Q (2019) A ratiometric fluorescence probe based on carbon dots for discriminative and highly sensitive detection of acetylcholinesterase and butyrylcholinesterase in human whole blood. Biosens Bioelectron 131:232–236

29. Wen Q, Zhu C, Liu L, Yang Q, Wang S, Zhu D (2012) Synthesis of a bifunctional fluorescent polymer for cell imaging and enzyme detection. Macromol Chem Phys 213:2486–2491

30. Lin M, Zou H, Yang T, Liu Z, Liu H, Huang C (2016) An inner filter effect based sensor of tetracycline hydrochloride as developed by loading photoluminescent carbon nanodots in the electrospun nanofibers. Nanoscale 8:2999–3007

31. Buss H, Chan TP, Sluis KB, Domigan NM, Winterbourn CC (1997) Protein carbonyl measurement by a sensitive ELISA method. Free Radic Biol Med 23:361–366

32. Li H, Yao Q, Xu F, Xu N, Duan R, Long S, Fan J, Du J, Wang J, Peng X (2018) Imaging γ-glutamyltranspeptidase for tumor identification and resection guidance via enzyme-triggered fluorescent probe. Biomaterials 179:1–14

33. Su L, Li P, Lu T, Mao C, Ji D, Hao M, Huang Z (2019) Protective effect of *Schisandra chinensis* total lignans on acute alcoholic-induced liver injury related to inhibiting CYP2E1 activation and activating the Nrf2/ARE signaling pathway. Rev Bras 29(2):198–205

34. Pereira C, Barros L, Ferreira IC (2016) Extraction, identification, fractionation and isolation of phenolic compounds in plants with hepatoprotective effects. J Sci Food Agric 96:1068–1084